Available online at www.sciencedirect.com
SCIENCE DIRECT
Coastal Engineering 53 (2006) 265 – 275
Coastal Engineering
An International Journal for Coastal, Harbour and Offshore Engineers
www.elsevier.com/locate/coastaleng

Simulating offshore sand waves

A.A. Németh [a,*], S.J.M.H. Hulscher [a], R.M.J. Van Damme [b]

[a] Department of Civil Engineering, University of Twente, P.O. BOX 217, 7500 AE Enschede, the Netherlands
[b] Department of Applied Mathematics, University of Twente, P.O. BOX 217, 7500 AE Enschede, the Netherlands

Available online 28 November 2005

Abstract

Sand waves form a prominent regular pattern in the offshore seabeds of sandy shallow seas and pose a threat to a range of offshore activities. A two-dimensional vertical (2DV) flow and morphological simulation model describing the behaviour of these sand waves has been developed. The simulation model contains the 2DV shallow water equations, with a free water surface and a general bed load formula. The water movement is coupled to the sediment transport equation with a seabed evolution equation. The domain is non-periodic in both directions. The spatial discretisation is performed by a spectral method based on Chebyshev polynomials. A fully implicit method is chosen for the discretisation in time. Firstly, we validate the simulation model mathematically by reproducing the results obtained using a linear stability analysis for infinitely small sand waves. Hereby, we investigate a steady current situation induced by a wind stress applied at the sea surface. The bed forms we find have wavelengths in the order of hundreds of metres when the resistance at the seabed is relatively large. The results show that it is possible to model the initial evolution of sand waves with a numerical simulation model. This paper forms the necessary first step to investigate the intermediate term behaviour of sand waves.

Keywords: Stability analysis; Numerical analysis; Spectral method; Sand waves; Generation; Shelf seas; 2DV

1. Introduction

Large parts of shallow seas—such as the North Sea—are covered with bed features having a variety of spatial dimensions (Fig. 1). Sand waves form a prominent bed pattern with a crest to crest spacing of hundreds of metres. Sand waves are observed at water depths in the order of 30 m and their heights can reach up to several metres. The crests are often assumed oriented perpendicularly to the principal current (Johnson et al., 1981; Langhorne, 1981). Based on a theoretical analysis, Hulscher (1996) showed that sand wave crests may deviate up to 10° anti-clockwise perpendicularly from the principal direction of the current on the northern hemisphere.

An analysis of the sand market Peters et al. (2001) showed that a shortage of sand is expected in the future in the Netherlands. The crests of sand waves are assumed to have the best composition for use in concrete. Knaapen and Hulscher (2002) showed that when a sand wave is dredged, it is able to recover in only a matter of years. This implies that small scale sand mining can be of a temporary nature only. Moreover, the behaviour of sand waves plays an important role in the selection of areas for large-scale sand extraction pits and their design. The influence of a pit or artificial island on its surrounding bed topography (including sand waves) is still unclear. Besides, the presence of sand waves changes the hydrodynamics and therefore the recolonization possibilities of benthic fauna (Stolk, 2000). Observations suggest that sand waves are dynamic (see for instance Allen, 1980b; Lanckneus and De Moor, 1991; Morelissen et al., 2003) and may migrate with speeds of up to several metres per year, which may cause buried pipelines to become exposed (Fig. 1). Therefore, insight into the behaviour of these sand waves is crucial to enable cost-effective management practices.

Huthnance (1982) was the first to look at a system consisting of depth-averaged tidal flow and an erodible seabed using a linear stability analysis. Within this framework, it is possible to investigate whether certain regular patterns develop as free instabilities of the system. Unstable modes comparable

* Corresponding author. Current address: Witteveen+Bos, Consulting Engineers B.V., P.O. Box 233, 7400 AE Deventer, the Netherlands.
E-mail addresses: a.nemeth@witbo.nl (A.A. Németh), s.j.m.h.hulscher@utwente.nl (S.J.M.H. Hulscher), r.m.j.vandamme@utwente.nl (R.M.J. Van Damme).

0378-3839/$ - see front matter © 2005 Elsevier B.V. All rights reserved.
doi:10.1016/j.coastaleng.2005.10.014

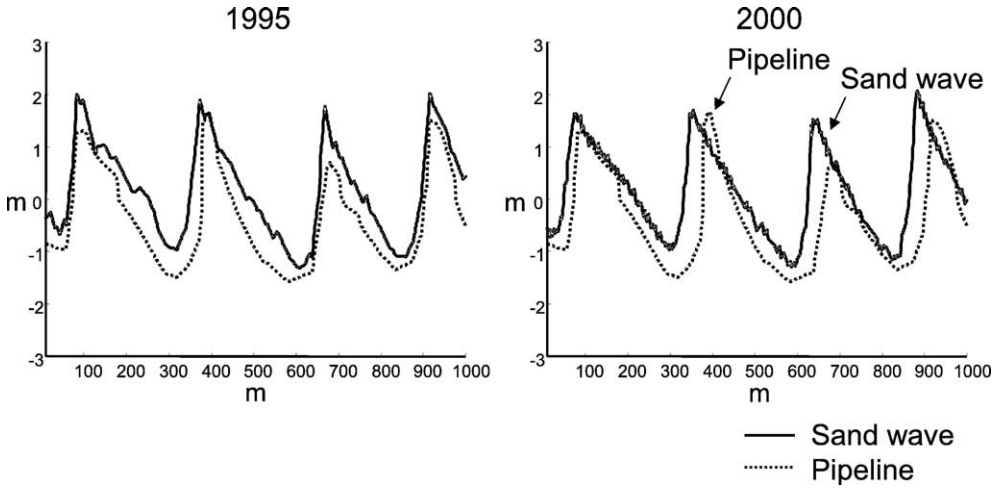

Fig. 1. Sand wave migration and pipelines. The solid line denotes the position of the seabed. The dotted line shows the position of the estimated pipeline. The measurements for two years (1995 and 2000) are shown. We can see that the sand wave is migrating to the left here, thereby exposing the buried pipeline (Courtesy Holland Offshore Consulting and State Supervision of Mines).

to tidal sandbanks were found, whereas smaller modes corresponding to sand waves were not initiated. This work was extended by Hulscher (1996) using a model allowing for vertical circulations and found formation of sand waves based on a horizontally averaged symmetrical tidal motion. The work showed that net convergence of sand can occur at the top of the sand waves over an entire tidal cycle (M2 tidal motion) (see also Gerkema, 2000; Komarova and Hulscher, 2000). Németh et al. (2002) extended the previous work by including an asymmetric basic flow (M0), inducing sand wave migration. Furthermore, Besio et al. (2003, 2004) discussed the effect using a stability analysis of an M4 tidal constituent on top of the M0 and M2 components.

A consequence of linear stability analyses is that their validity is limited to small-amplitude sand waves. However, this is far from the final aim, which is understanding the entire evolutionary process of sand wave formation. Komarova and Newell (2000) have extended the linear analysis by Komarova and Hulscher (2000) into the weakly non-linear regime for investigation of the behaviour of finite-amplitude idealised sand waves. However, migration is not considered. Fredsøe and Deigaard (1992) describe the behaviour of existing finite-amplitude dunes under a steady current. They assume the time dependence of the flow to be negligible when modelling sand waves in a tidal environment. Johns et al. (1990) discuss the finite amplitude behaviour of bed forms similar to sand waves under a steady current.

Numerical methods are a tool to overcome the limitations of a linear analysis and enable the study of the non-linear behaviour of these bed sand waves. This enables the description of the entire evolutionary process of sand waves and might give a clue to the most important mechanisms, determining the growth and stabilisation of sand waves. Furthermore, migration and irregular sand wave shapes can be further investigated (See Németh, 2003).

Software packages like Delft3D-MOR and Telemac form promising tools for future research. However, they are complex making it difficult to interpret the results and modify the model set up if necessary. Furthermore, a fully 3D morphological version of Delft3D-MOR (not depth-integrated) has only become available recently. Therefore, we developed a new simulation model, with the specific purpose of simulating offshore sand waves. Herein, we only incorporated the essential processes and focussed on the required accuracy to describe the vertical circulation cells responsible for the formation and long term evolution of offshore sand waves.

Within this paper, we focus on the first step, which is to reproduce the results obtained using a linear stability analysis for small amplitude sand waves Németh et al. (2002) (from here on referred to as “stability analysis”) with the new numerical simulation model (from here on referred to as “simulation model”). Hereby, we will focus on sand waves in a unidirectional steady current.

Firstly, we present the mathematical formulation of the sand wave simulation model. It is based on the two-dimensional vertical shallow water equations combined with a simple sediment transport equation, describing bed load transport. Next, the numerical set-up pursued in this work is discussed. We present the coordinate transformation method, the spatial and temporal discretisation. Subsequently, we validate the simulation model mathematically by comparing it with the linear stability analysis discussed in Németh et al. (2002). In the final section, we present the discussion and conclusions.

2. 2DV morphological model

2.1. Flow model

The simulation model presented in this paper is based on Németh et al. (2002). It is known that the Coriolis force only slightly affects sand waves Hulscher (1996). Therefore, the behaviour of sand waves can be described with the help of the

two-dimensional vertical (2DV) model. We start from the 2DV shallow water equations:

$$\frac{\partial u}{\partial t} + u\frac{\partial u}{\partial x} + w\frac{\partial u}{\partial z} = -g\frac{\partial \zeta}{\partial x} + \frac{\partial}{\partial z}\left(A_v \frac{\partial u}{\partial z}\right), \quad (1)$$

$$\frac{\partial u}{\partial x} + \frac{\partial w}{\partial z} = 0. \quad (2)$$

The symbols g and A_v indicate the acceleration due to gravity and the vertical eddy viscosity, respectively. Time is represented by t. The velocities in the x- and z- directions are u and w, respectively. The water level is denoted by ζ and H represents the mean water depth. The level of the seabed is represented by $-H+h$ (see Fig. 2).

2.2. Sediment transport and seabed behaviour

The sediment transport model in this paper describes bed load transport. This mode of transport is assumed to be dominant in offshore tidal regimes (See also Besio and Blondeaux, 2003). As the velocity distribution over the water column is calculated explicitly, bed load transport can be modelled as a function of the shear stress at the seabed. This is in contrast with depth-averaged models, which calculate the sediment transport as a function of the depth-averaged velocity. The following general volumetric bed load formula for S_b is used, following Komarova and Hulscher (2000):

$$S_b = \alpha|\tau_b|^b\left[\tau_b - \lambda_1\frac{\partial h}{\partial x} - \lambda_2|\tau_b|\frac{\partial h}{\partial x}\right], \quad (3)$$

with τ_b the shear stress at the seabed:

$$\tau_b = A_v\frac{\partial u}{\partial z}\bigg|_{z=-H+h}. \quad (4)$$

The power of transport (b) is set at 1/2. The proportionality constant α is set at a value of 0.3 s m^{-2} following Van Rijn (1993) and incorporates the density difference between water and sediment. The first scale factor for the bed slope mechanism (λ_1) and the second scale factor λ_2 take directly into account that sand is transported more easily downhill than uphill. The default values of λ_1 and λ_2 are set at 0.002 m^2 s^{-2} and 3.33, respectively. In the stability analysis Németh et al. (2002), λ_1 and λ_2 were taken together (i.e. $\lambda=\lambda_1+\lambda_2|\tau_b|_{z=-H}$) since both terms in that case contribute in the same manner since $h \ll H$. In this study, a threshold of sediment motion is not taken into account explicitly.

The sediment balance, which couples the flow model Eqs. (1) and (2) with the sediment transport model Eq. (3), calculates the position of the seabed based on the principle of conservation of mass as a function of time:

$$\frac{\partial h}{\partial t} = -\frac{\partial S_b}{\partial x}. \quad (5)$$

The bed level will hardly vary on a tidal timescale.

2.3. Boundary conditions and assumptions

The boundary conditions at the water surface ($z=\zeta$) are given as follows:

$$\frac{\partial \zeta}{\partial t} + u\frac{\partial \zeta}{\partial x} = w, \quad (6)$$

$$\frac{\partial u}{\partial z} = \frac{\tau_w}{A_v}. \quad (7)$$

in which τ_w describes the wind induced shear stress at the sea surface. The vertical velocity component at the seabed ($z=-H+h$) is described by the kinematic condition:

$$\frac{\partial h}{\partial t} + u\frac{\partial h}{\partial x} = w. \quad (8)$$

The horizontal flow components at the seabed are modelled with the help of a partial slip condition (S is the resistance parameter controlling the resistance at the seabed). The boundary condition couples the resistance at the seabed with the water movement across the seabed:

$$A_v\frac{\partial u}{\partial z} = Su. \quad (9)$$

A comprehensive discussion on the parameter S and its relation to observed bed forms can be found in Hulscher and Van den Brink (2001) and Besio et al. (2004).

Furthermore, we use non-periodic boundary conditions in the horizontal and vertical direction. This set up also gives more freedom to the system with respect to the selection of the fastest growing mode. In a periodic set up, the amount of modes which can be unstable is limited by the horizontal length of the grid, since we pose a limitation on the wavelength the simulation model is allowed to select. Since we are also interested in the behaviour of the wavelength of a sand wave during its evolution, we keep the simulation model set up as generic as possible.

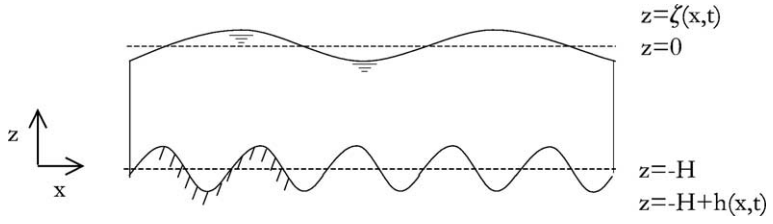

Fig. 2. Definition sketch of the non-periodic dimensional model geometry of the physical domain. The horizontal and vertical direction are denoted by x and z. The water surface is defined by ζ relative to $z=0$. The seabed is defined as h and is relative to the average seabed position, $-H$.

At the inflow boundary, a discharge is prescribed, with a certain velocity profile in the vertical plane. In case of a steady flow, two possible origins are investigated in Németh et al. (2002). These are (I) a wind driven current (τ_w) and (II) a current induced by a pressure gradient. The vertical structure for each of these cases is:

$$\text{I}: \quad u_r = \frac{\tau_w}{A_v}\left(H + \frac{A_v}{S} + z\right), \tag{10}$$

$$\text{II}: \quad u_r = P\left(\frac{1}{2}z^2 - \frac{A_v}{S}H - \frac{1}{2}H^2\right), \tag{11}$$

with P a parameter determining the magnitude of the pressure gradient and thereby the depth-averaged velocity. These profiles are equivalent to the analytical expressions of the basic state situation over a flat seabed used in the stability analysis with the seabed positioned at $z=-H+h$. In this paper we will only focus on the effect of a wind driven current.

The outflow boundary is physically an open boundary. However, the simulation model requires a boundary condition. Therefore, an estimate of the water level is supplied to the simulation model at the outflow boundary. Furthermore, the derivatives in the horizontal direction for the horizontal and vertical velocities are set to zero at the outflow boundary.

2.4. Discussion boundary conditions

Even though we are setting up the simulation model in a non-periodic way, we investigate the possibility of applying periodic conditions. Periodic boundary conditions provide the main benefit of simplifying the system, decreasing calculation time. Since the outflow and inflow boundary are then the same, no extra physical space needs to be reserved near the boundaries, avoiding the problem of physical disturbances reaching the boundaries and reflecting.

A wind stress applied at the sea surface (Eqs. (10) and (7)) is balancing the resistance in the system equally over the entire domain. This forcing mechanism induces water movement without a gradient in the water level for a flat seabed. The water level and velocity profile at the outflow boundary are therefore the same as the inflow boundary (when the position and gradient of the seabed are the same at both boundaries). Therefore, it is also possible to use periodic boundary conditions in the horizontal direction. Obviously, the vertical direction always has to remain non-periodic.

When we apply a pressure gradient at the inflow boundary Eq. (11), the water level decreases moving away from the inflow boundary, due to resistance in the domain. Due to continuity (Eq. (2)), the depth-averaged velocity increases along the reducing water level. Therefore, the velocity profiles, water and seabed levels at the in and outflow boundary can never coincide. Tidal motion can be approached as a time-dependent pressure gradient at the inflow boundary. Therefore, in the set up of applying periodic boundary conditions, the entire tidal wave needs to be described. In practice, this is not feasible, since we require accurate results for a relative small length scale (sand waves with a wavelength of hundreds of metres compared to the wavelength of a tidal wave of hundreds of kilometres). However, periodic boundary conditions are also here possible in the case of a pressure gradient if we incorporate the pressure gradient directly in the momentum equation Eq. (1). Then, the simulation model still contains a free surface, which responds to variations in the seabed. However, no gradient is present in the case of a flat seabed, making periodic boundary conditions possible.

3. Numerical approximation

3.1. Spatial discretisation

A spectral collocation method is used to obtain a discrete approximation of the equations of the solution, on a set of discrete grid points (Canuto et al., 1988; Fornberg, 1996). This method is applied in both coordinate directions. The discrete grid points are specified by collocation points. The grid points are given by the most commonly used Chebyshev Gauss–Lobatto points:

$$\xi^k = \cos\left(\frac{\pi j}{N}\right), \quad \text{with} \quad j = 0, 1, \ldots, N^k \quad \text{and} \quad k = 1, 3. \tag{12}$$

The collocation method implies that the residual function is forced to zero at these points. N^k defines the number of intervals in the ξ^k-direction. The solution is represented at each grid point using one-dimensional basis functions. The basis functions consist of the Chebyshev polynomials (T_p) defined by:

$$T_p(Z) = \cos\left(p\ \cos^{-1}(Z)\right), \quad \text{with} \quad p = 1, 2, \ldots \tag{13}$$

For the grid points, the Chebyshev collocation derivative can be obtained in two different ways. The first method is to calculate the derivatives in spectral space (transform method). This method involves three steps. Firstly, a Discrete Chebyshev Transform has to be applied, after which differentiation can take place in spectral space. The solution then has to be transformed back to physical space using the Inverse Discrete Chebyshev Transform.

The second method—differentiation in physical space—combines the three steps of the transform method. This results in a matrix **D** given by Canuto et al. (1988), which can be used to calculate the first derivative at the grid points:

$$\mathbf{D}_{ij} = \begin{cases} \frac{c_i^{i+j}}{c_j x_i - x_j}, & i \neq j \\ \frac{-x_j}{2\left(1-x_j^2\right)}, & 0 < i = j < N \\ -\frac{2N^2+1}{6}, & i = j = 0 \\ \frac{2N^2+1}{6}, & i = j = N. \end{cases} \tag{14}$$

where

$$c_j = \begin{cases} 2, & j = 0 \text{ or } j = N \\ 1, & 1 \leq j \leq N-1. \end{cases} \tag{15}$$

The matrix necessary to calculate a second derivative at the grid points can be calculated by taking the square of matrix **D** given in Eq. (14). The vector containing the function values U at the collocation points is multiplied with this first or second derivative matrix to obtain a vector containing the values for the first or second derivative values at the collocation points, respectively. The two-dimensional version of Eq. (14) in the horizontal and vertical direction can be found in the Appendix in Eqs. (40) and (41).

3.2. Coordinate transformation

A coordinate transformation is required allowing for a smooth description of the seabed topography together with a varying water surface on the computational grid. This transformation will allow the total number of collocation points to remain the same irrespective of the local water depth.

The coordinate system used for the computational space is represented by ξ^1 for the horizontal direction and ξ^3 for the vertical direction (see also Fig. 3). Both directions of the computational coordinate system have a domain of $[-1,1]$ to coincide with the Gauss–Lobatto grid. This system is obtained by mapping the physical space, represented by the Cartesian coordinates x and z, with the following analytical transformations:

$$\xi^1 = 1 - \frac{2x}{N_{sw}L_{sw}}, \tag{16}$$

$$\xi^3 = 1 - \frac{2(z-\zeta)}{\zeta + H - h}, \tag{17}$$

with L_{sw} the initial wavelength of the sand wave chosen to be investigated with the simulation model and N_{sw} the number of sand waves in the domain. The total length of the domain is therefore N_{sw} times the wavelength L_{sw}.

3.3. Partial derivatives

Next, we compute the necessary partial derivatives for (ζ, h, u, w), to compensate for the changes in physical space projected on the fixed computational grid and η the computational time:

$$\frac{\partial u}{\partial x} = \frac{\partial u}{\partial \xi^1}\frac{2}{N_{sw}L_{sw}} + 2\frac{\partial u}{\partial \xi^3}\frac{\zeta_x - \frac{1}{2}\left(\xi^3 - 1\right)\left(\zeta_x - h_x\right)}{\zeta + H - h}, \tag{18}$$

$$\frac{\partial u}{\partial z} = \frac{\partial u}{\partial \xi^3}\frac{2}{\zeta + H - h}, \tag{19}$$

$$\frac{\partial^2 u}{\partial z^2} = \frac{\partial^2 u}{\partial \xi^{3^2}}\left\{\frac{2}{\zeta + H - h}\right\}^2, \tag{20}$$

$$\frac{\partial u}{\partial t} = 2\frac{\partial u}{\partial \xi^3}\frac{\partial \zeta}{\partial t}\frac{1 - \frac{1}{2}\left(\xi^3 - 1\right)}{\zeta + H - h} + \frac{\partial u}{\partial \eta}. \tag{21}$$

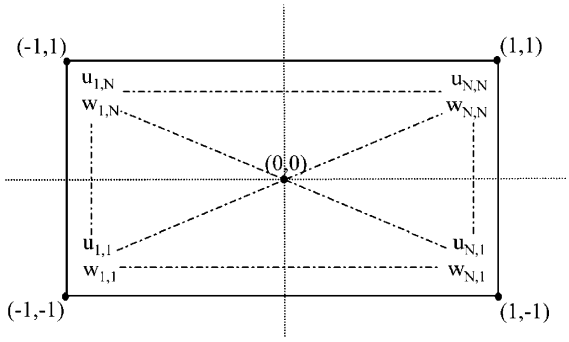

Fig. 3. Computational grid and indices used in the code.

The necessary partial derivatives for the other variables w, h and ζ can be derived in a similar manner.

3.4. Temporal discretisation flow model and grid

The spatial approximation using a Chebyshev grid is the best in the interior of the domain. Therefore, an increased density of grid points is required near the boundaries. The numerical convergence rate of the method decreases significantly if this is not the case. This aspect has an effect on the choice of the time scheme. An explicit scheme is desirable, with respect to the computational effort necessary per time step. However, the size of the time step, is determined by the smallest distance between grid points in the domain. Therefore, a higher density of grid points near the boundaries—as with the Gauss–Lobatto grid—poses a problem. If we increase the total number of grid points, the smallest distance between grid points will decrease more than the relative increase in points. The time step will become too small to be efficient.

The most practical approach is therefore to use a fully implicit formulation. In this case the time step does not depend anymore on the spatial discretisation for stability reasons. All the properties of u, w, ζ and h are calculated simultaneously at each time step. The calculation cost per time step is higher than for an explicit formulation. However, the time steps that can be taken are much larger (See also Stelling et al. (1998)).

The system is solved with the routine D02NGF from the Nag libraries. It is a general-purpose routine, which can integrate initial value problems, for a stiff system of ordinary differential equations, with coupled algebraic equations. The system is written in the form:

$$\mathbf{A}(t, \boldsymbol{Y})\frac{d\boldsymbol{Y}}{dt} = r(t, \boldsymbol{Y}), \tag{22}$$

with $\boldsymbol{Y}=(u, w, \zeta, h)$ the solution vector. On the left hand side, we find the derivatives of the solution vector $\boldsymbol{Y}$. Matrix **A** can be found in the Appendix Eq. (42).

On the right hand side, their dependency on time can be found. Here, the differential equations and boundary conditions, which do not have a time-dependent term, appear as the residuals of the continuity equation (Eq. (2)). When the right hand side is zero, we are looking at a steady state solution. If it is non-zero, the solution is changing in time.

The momentum balance Eq. (1) containing the temporal discretisation in the form of Eq. (22) can be written as follows:

$$\frac{\mathrm{d}u}{\mathrm{d}t} = -2\frac{\partial\zeta}{\partial t}\frac{1-\frac{1}{2}\left(\xi^3-1\right)}{\zeta+H-h}\mathbf{D}_1^3u - \frac{2}{N_{\mathrm{sw}}L_{\mathrm{sw}}}u\mathbf{D}_1^1u - 2\frac{\zeta_x-\frac{1}{2}\left(\xi^3-1\right)(\zeta_x-h_x)}{\zeta+H-h}u\mathbf{D}_1^3u + \frac{2}{\zeta+H-h}w\mathbf{D}_1^3u - g\frac{2}{N_{\mathrm{sw}}L_{\mathrm{sw}}}\mathbf{D}_1^1\zeta + A_{\mathrm{v}}\left(\frac{2}{\zeta+H-h}\right)^2\mathbf{D}_2^3u. \quad (23)$$

Here $\mathbf{D}_k^i$ is the k-th derivative in the i-th direction. The partial derivatives h_x and ζ_x are of the form of Eq. (18).

The continuity equation (Eq. (2)) is an instantaneous constraint that applies at each time level and can be found on the right hand side of Eq. (22) as a time independent equation:

$$\frac{2}{N_{\mathrm{sw}}L_{\mathrm{sw}}}\mathbf{D}_1^1u + 2\frac{\zeta_x-\frac{1}{2}\left(\xi^3-1\right)(\zeta_x-h_x)}{\zeta+H-h}\mathbf{D}_3^1u - \frac{2}{\zeta+H-h}\mathbf{D}_1^3w = 0. \quad (24)$$

At the inflow boundary Eqs. (10) and (11) we find:

$$u = \text{prescribed}|_{x=-1} \quad \text{and} \quad w = 0|_{x=-1}. \quad (25)$$

At the outflow boundary, we find the horizontal derivatives of u and w set to zero, resulting in:

$$\frac{2}{N_{\mathrm{sw}}L_{\mathrm{sw}}}\mathbf{D}_1^1u + 2\frac{\zeta_x-\frac{1}{2}\left(\xi^3-1\right)(\zeta_x-h_x)}{\zeta+H-h}\mathbf{D}_1^3u = 0|_{x=1}, \quad (26)$$

$$\frac{2}{N_{\mathrm{sw}}L_{\mathrm{sw}}}\mathbf{D}_1^1w + 2\frac{\zeta_x-\frac{1}{2}\left(\xi^3-1\right)(\zeta_x-h_x)}{\zeta+H-h}\mathbf{D}_1^3w = 0|_{x=1}. \quad (27)$$

Furthermore, the water level is fixed at the downstream boundary. The boundary condition at the free surface can now be written as a kinematic condition Eq. (6), together with a shear stress at the surface equal to the wind stress Eq. (7) (if present):

$$\frac{\partial\zeta}{\partial\eta} + u\frac{2}{N_{\mathrm{sw}}L_{\mathrm{sw}}}\mathbf{D}_1^3\zeta = w|_{z=\zeta}, \quad (28)$$

$$-\frac{2}{\zeta+H-h}\mathbf{D}_1^3 = \tau_{\mathrm{w}}|_{z=\zeta}. \quad (29)$$

At the seabed we find another kinematic condition Eq. (8) and the partial slip condition Eq. (9):

$$w - u\frac{2}{N_{\mathrm{sw}}L_{\mathrm{sw}}}\mathbf{D}_1^1h = 0|_{z=-H+h}, \quad (30)$$

$$u - \frac{2}{\zeta+H-h}\frac{A_{\mathrm{v}}}{S}\mathbf{D}_1^3u = 0|_{z=-H+h}. \quad (31)$$

The sediment transport model Eq. (3) in discretised form can be written as:

$$S_{\mathrm{b}} = \alpha|\left(\frac{2}{\zeta+H-h}\right)^2\mathbf{D}_1^3u|^b \left[\mathbf{D}_1^1u - (\lambda_1+\lambda_2|\tau_{\mathrm{b}}|)\frac{\zeta+H-h}{N_{\mathrm{sw}}L_{\mathrm{sw}}}\mathbf{D}_1^1h\right], \quad (32)$$

with τ_{b} the shear stress at the seabed defined by Eq. (4). The net inflow of sediment is assumed to be zero. The seabed evolution Eq. (5) can now be described on the computational grid by:

$$\frac{\partial h}{\partial t} = \frac{2}{N_{\mathrm{sw}}L_{\mathrm{sw}}}\mathbf{D}_1^1S_{\mathrm{b}}. \quad (33)$$

For completeness, we have to specify a boundary condition at a boundary coinciding with the horizontal position of the flow boundaries for the bottom evolution equation. This is equivalent to the boundary condition necessary for the water level. This can also be done by taking the derivative of the sediment transport equal to zero coinciding with a fixed seabed. At this point, only the initial response is needed here for comparison with the results from the stability analysis.

3.5. Initial values and time stepping

For a flat seabed, the initial conditions can be derived analytically. In case the seabed is not flat, but contains for example a sinusoidal feature, we cannot use the solution for a flat seabed. However, we can use it as an estimate for the required initial condition. A better initial condition can be given by the solution of the stability analysis, which is valid for infinitesimal amplitudes ($h \ll H$) (Németh et al., 2002).

The estimates of the initial solution prescribed using these two approaches for a finite sinusoidal sand wave are not the exact solutions of the system. This difference in applied solution and the actual solution can be seen as an initial disturbance in the system. The order of magnitude of the error/disturbance depends on the ratio of h/H, the spatial discretisation and the requested accuracy from the time integrator.

The propagation velocity c of a wave in shallow water is calculated with:

$$c = \sqrt{gH} \quad (34)$$

A steady state solution, which we in general require to start a simulation, can be achieved by letting the disturbances travel through the domain a couple of times. For a typical water depth of 30 m, the propagation velocity is about 17 m s^{-1} according to Eq. (34). For a domain with a length of 2 km, this would mean that a disturbance in the water motion due to the incorrect initial solution takes about 120 s to travel from one end of the domain to the other. After about 600 s we can expect a virtually steady state solution. This solution can then form the starting point for a simulation.

In the limit ($t\to\infty$) the changes in time for a steady state solution should be equal to zero. Therefore, the residuals of Eq.

(22) are practically zero which is discussed below. Furthermore, this aspect can be seen by looking at the magnitude of the time step of the time integrator. This time step is small initially due to the calculation of all the dependencies of the system and possible initial changes in the physical system. Large time steps can be taken when the steady state situation has been attained, as long as the seabed does not change.

When the seabed is allowed to change, the magnitude of the time step becomes a function of this seabed change. The time steps are then still large due to the slow evolution of the seabed compared to the water movement, in case of a steady state current. This is due to the difference in timescale for the water motion and seabed change. This only holds for the case of a steady current or a block current. In the case of pure tidal motion, the time step size is again determined by the timescale of the water motion. However, here we will first investigate if we can reproduce the initial response of applying a seabed perturbation using a simulation model.

4. Results

We start with the investigation of a steady flow. First, we discuss in short this steady flow and its effects on the behaviour of the seabed with the help of a stability analysis. The steady flow is assumed to be induced by a wind stress applied at the sea surface. Next, we show that the results from the simulation model coincide with the stability analysis.

4.1. Steady flow and sand waves according to a stability analysis

We start by focussing on a unidirectional steady current inducing the initial evolution of bed forms. The bed forms we find in this case can also be referred to as dunes [Fredsøe and Deigaard, 1992], since a unidirectional steady current is similar to river flow. For typical values of the resistance parameter S in the North Sea (see Table 1), we find long wavelengths (see Fig. 4). Hereby, we used in the stability analysis a combined non-dimensional value for λ_1 and λ_2 (Eq. (3)):

$$S_b = \alpha|\tau_b|^b\left[\tau_b - \lambda\frac{\partial h}{\partial x}\right] \quad \text{with } \lambda = \lambda_1 - \lambda_2|\tau_b|, \tag{35}$$

with λ equal to 0.0085. However, if we increase the value of the resistance parameter, we find shorter bed forms Németh et al. (2001) (See Figs. 4 and 6. The latter figure is discussed later in more detail.), with wavelengths of a couple of hundreds of metres. This coincides with the result found in Németh et al. (2002). In a tidal environment with a small asymmetry in the water motion, the tidal motion is the main factor determining the choice of sand wavelength. The residual currents due to tidal motion induce a wider range of modes which can become unstable than the unidirectional steady current. An increase in resistance can increase this range of modes, for which the wavelength of the fastest growing mode (FGM) is smaller (larger wave number). Here, the FGM is the mode which has the largest growth rate from linear theory, and is expected to dominate over the rest.

Table 1
Default values and dimensions of the parameters and variables existing in the system

Parameters	Symbol	Default value	Dimension
Depth-averaged value velocity	U	1	m s^{-1}
Average water depth	H	30	m
Kinematic eddy viscosity	A_v	$3\cdot10^{-2}$	m^2 s^{-1}
Resistance parameter	S	$1\cdot10^{-2}$	m s^{-1}
Gravitational acceleration	g	9.8	m s^{-2}
Power of transport	b	$5\cdot10^{-1}$	–
Proportionality constant	α	$3\cdot10^{-1}$	m^{-2} s
Bed slope factor	λ_1	$2\cdot10^{-3}$	m^2 s^{-2}
Bed slope factor	λ_2	3.33	–
Sand wavelength	L_{sw}	600	m
Number of sand waves	N_{sw}	3	–

4.2. Mathematical validation simulation model

4.2.1. Flat bed

We start with a steady current over a flat bed, which is equivalent to the basic state used in the stability analysis. We apply a wind stress at the sea surface (see Eq. (10) and Fig. 5) across a flat seabed together with a coinciding in flow boundary. The analytically obtained profile is the same over the entire domain. This investigation of a flat seabed shows the functionality of the continuity equation (Eq. (2)), the boundary conditions Eqs. (6)–(11) and the viscosity term in the momentum equation Eq. (1).

We investigate the magnitude of the residuals on the right hand side of Eq. (22), whether the solution coincides with the solution of the physical system. Since the solution provided is a steady state solution and the velocity in the vertical is zero (there is no slope in the seabed or water level), all the residuals on the right hand side of Eq. (22) should be zero within machine accuracy limits. The profile in the vertical can be found in Fig. 5.

If we would apply a pressure gradient at the inflow boundary, a gradient is present in the water surface due to the friction in the system. This is in contrast to the stability analysis, where the velocity profile is the same over the entire domain. This makes a direct comparison more difficult. However, this can also be seen as a good test for the simulation model and the usage of the basic state in the stability analysis.

We can take an initial condition for a flat seabed and an equal velocity profile over the entire domain equal to inflow boundary for a pressure gradient Eq. (11). If we fix the water level downstream ($z=0$) and fix the depth-averaged velocity at the inflow boundary, we obtain a steady state solution with a slope in the water level. The continuity equation enforces the depth-averaged velocity to increase along this decreasing slope. This slope decreases $8.45\cdot10^{-3}$ m per 10 km for a standard value of the resistance parameter S of $1\cdot10^{-3}$ m s^{-1} (see Table 1). In case we are looking at bed forms in a unidirectional steady current, the typical value for S is $1\cdot10^{-2}$ m s^{-1} and gives a slightly larger slope of $1.46\cdot10^{-2}$ m per 10 km. This slope is so small compared to the length scale under investigation, that we can assume the validity as expected of the basic state used in the stability analysis.

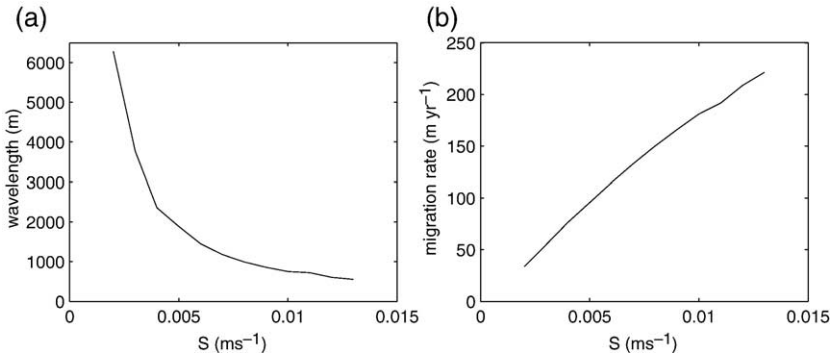

Fig. 4. Wavelength and migration rate in a unidirectional steady current induced by a wind stress applied at the sea surface. Fig. (a) shows the wavelength (m) of the fastest growing mode (FGM) as a function of the value of the resistance parameter S (m s^{-1}). Fig. (b) shows the migration rate in metres of the FGM shown in (a). If we increase the value of the resistance parameter S we obtain sand waves with dimensions in the order of hundreds of metres.

4.2.2. Residuals solution for small amplitude sand waves

The question to be answered is whether the formation process of small amplitude sand waves can be reproduced and verified with a simulation model. To check this we use the results obtained with the stability analysis. The vertical velocity is zero for a flat bed situation. The vertical velocity to be imported in the simulation model is equal to the calculated vertical velocity in the perturbed state in the stability analysis. The sum of the residual horizontal velocity and the basic state forms the actual horizontal velocity with sand waves applied on the seabed. These results, produced on an equidistant grid, are interpolated on the Gauss–Lobatto grid, using cardinal polynomials.

The time derivative is equivalent to the residuals in Eq. (22). For the other equations, the magnitude of the residuals, is a measure for the error. To check the validity of the spatial discretisation, we therefore do not need to use the time integrator. The results for a wavelength of 600 m are imported in the simulation model (See Fig. 6). The solution of the stability analysis is multiplied by $\epsilon = h/H$. For a small enough ε, the solution from the simulation model is equal to the solution from the stability analysis (residuals equal zero within numerical accuracy, with a difference of the order (ϵ^2).

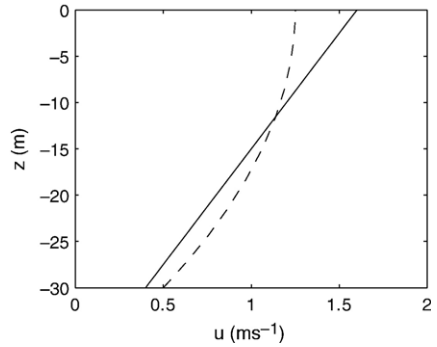

Fig. 5. Analytical solution of the horizontal velocity profile over a flat bed in case of a wind stress applied at the sea surface (straight solid line) Eq. (10) and a pressure gradient (curved dotted line) Eq. (11). The linearity of the velocity profile in case of a wind stress is due to the choice of a constant viscosity. The free surface coincides with $z = 0$ m and the seabed with $z = -30$ m. The vertical velocity is equal to zero. This profile is applied at the inflow boundary for all times (with a fixed or time-dependent discharge) and as initial condition over the entire domain.

4.2.3. Growth and migration

As a final check, we allowed the simulation model to determine a seabed change over a period of 7000 s. This is a small time interval, insignificant from a morphological perspective. However, from a mathematical point of view sufficient, since the aim is here to check the mathematical validity of the simulation model. We applied again a steady flow induced by a wind stress. With the system set up following the values in Table 1, except for the value of the resistance parameter which is equal to 0.01 m s^{-1}. Furthermore, we used the same combined bed slope factor as was used above (Eq. (3)) for comparison. Moreover, we took $N^1 = 30$ and $N^3 = 15$, which are the number of grid points in the horizontal and vertical direction (Eq. (12)), respectively. The amplitude h is set at 0.01 m, which is small compared to the water depth H of 30 m. Hereby, we investigated a pattern of three sand waves in a non-periodic domain.

We calculated the growth and migration rates, for a whole range of wavelengths. We use a least squares method, to estimate the growth and migration rates based on the initial and calculated seabed obtained with the simulation model. This curve fitting process is used to fit a sinus with a minimal deviation to the position of the seabed, with sinusoidal sand waves imprinted on it, in the grid points. Here we investigate the initial response. Therefore, we are allowed to assume the wavelength does not change, and only the amplitude and position in the horizontal (phase/migration) changes. This approach gives an estimate of the amplitude and phase of a sinusoidal signal, in this case the sand wave. This coincides with the properties the stability analysis gives insight into (growth and migration of a sinusoidal sand wave), which we are comparing the results with. These properties of the imposed sand waves and resulting bed pattern after the simulation period can now be determined as follows:

$$h(x) = A_{\mathrm{ls}}\cos(kx) + B_{\mathrm{ls}}\sin(kx), \tag{36}$$

with $h(x)$ the position of the seabed as a function of the horizontal coordinate and φ the phase shift defined by:

$$\varphi = a\tan\left(\frac{B_{\mathrm{ls}}}{A_{\mathrm{ls}}}\right), \tag{37}$$

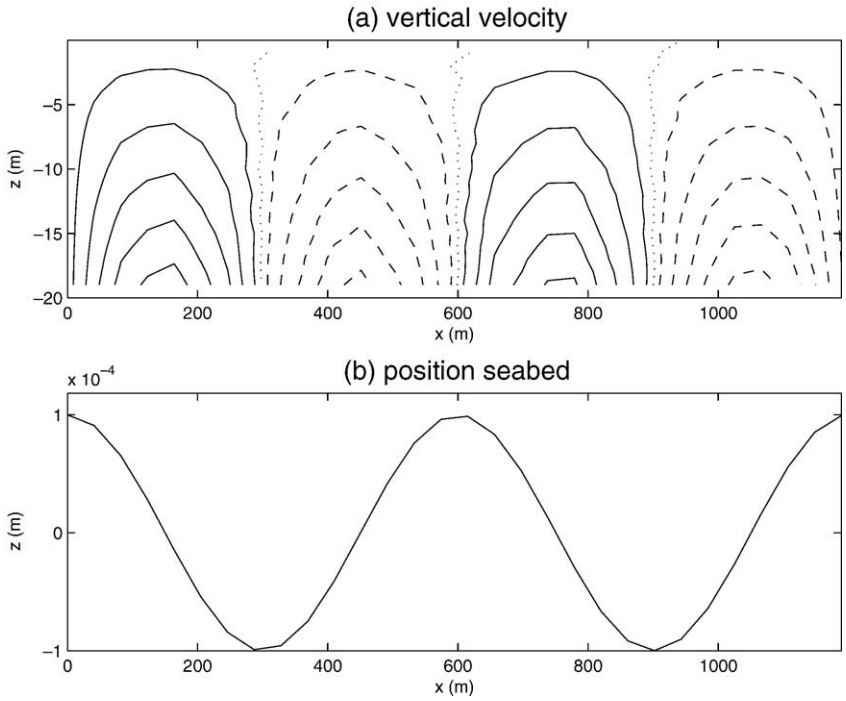

Fig. 6. Solution of the stability analysis giving residuals equal to zero in the simulation model. In the upper figure (a), the vertical velocity is shown with the solid line showing negative, the dashed line positive and the dotted line velocities equal to zero. The magnitude of the velocities depends on the ratio of the sand wave amplitude over the water depth ($\epsilon = h/H$). The vertical velocity looks different from previous work discussing sand waves in a tidal environment. The main difference is that we are looking here at a steady current and not at the residuals over a tidal cycle. This means looking at the boundary condition for the horizontal flow Eq. (8), that the vertical velocity needs to follow the profile of the seabed. This is due to the occurrence of a horizontal velocity$\neq 0$, due to the horizontal viscosity model enabling long bed waves to be excited (there is evolution due to water movement, and the slope effect is very small for long bed forms). The figure below (b) shows the two sand waves with a typical wavelength of 600 m over which the water is flowing.

and A and B based on the depths at the grid points:

$$A_{\mathrm{ls}} = \frac{\sum h(x)\cos(kx)}{\sum \cos^2(kx)}, \tag{38}$$

$$B_{\mathrm{ls}} = \frac{\sum h(x)\sin(kx)}{\sum \sin^2(kx)}. \tag{39}$$

Fig. 7 shows the characteristics of the initial response for a range of wavelengths. Fig. 7a depicts the growth rates, whereby we find a range of wavelengths for which these growth rates are positive. For this range, sand waves are initially unstable. Furthermore, we find for all long bed waves positive growth rates. This is due to the usage of a constant viscosity. It can be explained by looking at the boundary conditions showing that the vertical velocity at the seabed is a function of the horizontal velocity at the seabed (Eqs. (8) and (9)). Both the horizontal and vertical velocity are therefore not equal to zero. This is due to the usage of a resistance parameter to obtain a more realistic shear stress with this simplified viscosity model. Smaller wavelengths than about 400 m show negative growth rates. These bed forms are dampened by the simulation model, as coincides with the results for this case with the stability analysis. Here, the FGM has a wavelength of

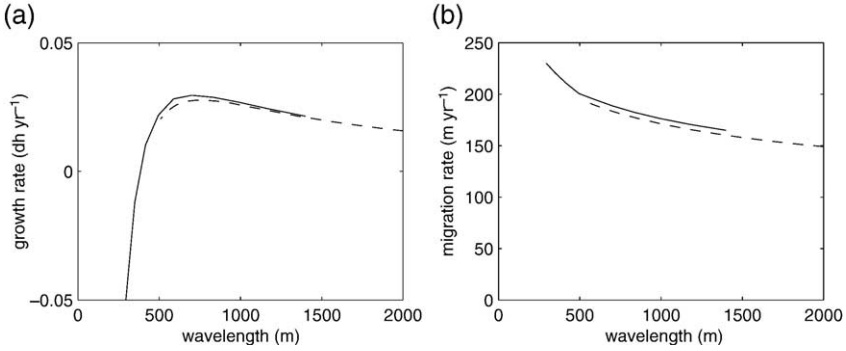

Fig. 7. Comparison growth and migration rates of the stability analysis and simulation model. Fig. (a) shows the initial growth rate presented in the change of amplitude per year (m yr^{-1}). Here we have to keep in mind that the growth rate is, according to the stability analysis, an exponential function of the amplitude. This means that the growth rate will increase during the initial evolution of a sand wave. The solid line depicts the results from the simulation model. The dotted line corresponds to the results from the stability analysis. Fig. (b) shows the migration rate (initial response calculated in m yr^{-1}).

about 750 m. Also this coincides with the results from the stability analysis.

The migration rate of the sand waves is shown in Fig. 7b. Typical rates for various wavelengths are about 200 m yr^{-1}. These migration rates are due to the asymmetry in the water motion since we are looking at a unidirectional steady current. Compared to observations these migration rates are much higher than those observed for sand waves. However, observations generally discuss sand waves in a tidal environment with only a small non-periodic part in the water motion (usually in the range of 0.1 m s^{-1} inducing migration rates in the order of 10 m yr^{-1} (Allen, 1980a; Lanckneus and De Moor, 1991; Van Maren, 1998; Németh et al., 2002). Therefore, these larger migration rates can be explained and give further confidence in the simulation model set up. As was found in the stability analysis, the phase speeds are a linear function of the wave number ($k=2\pi/L_{sw}$). This means that a larger wave number or smaller wavelength implies a larger phase speed. This results in a larger migration rate for smaller bed forms. The magnitude of this migration rate for a certain wavelength depends largely on the magnitude of the steady current and on the value of the resistance parameter S.

Before we compare the results of the stability analysis and the simulation model, we have to acknowledge a couple of sources of errors:

- The results from the stability analysis contain numerical inaccuracies;
- We are looking at a non-periodic domain in the simulation model and in the stability analysis we have a periodic domain;
- An error is made translating the results from the simulation model with the least square method, to enable a comparison with the stability analysis.

Therefore, it is not our goal to reproduce the results exactly. However, it is possible to obtain a result with the simulation model, which converges asymptotically to the result of the stability analysis, if we increase the accuracy of the time integrator, the number of nodes in the system (N^k in Eq. (12)) and the number of sand waves in the domain. To obtain Fig. 7, we already needed to increase the time integrators accuracy for smaller wavelengths, whereby the solution converged to the analytical solution. Furthermore, we found that if we increase the number of wavelengths in the domain from two to three, the difference with the stability analysis decreased from $5\cdot10^{-2}$ to $2\cdot10^{-2}$. The latter results (determined with a domain with three sand waves) are shown in Fig. 7.

5. Conclusions and discussion

In this paper we developed a numerical simulation model able to describe sand wave excitation and select the initially most unstable mode assuming sand waves are free instabilities of the water–seabed system. This model has been mathematically validated using an existing stability analysis.

In the stability analysis the sand waves predicted did not allow for interference of modes due to the linear assumption. This interference encompasses energy being transferred from one component or wave number of the bed pattern to another. Therefore, this stability analysis does not say anything about the final pattern, since only one component can be investigated at a time. The simulation model developed and validated mathematically here, can be used to investigate the non-linear behaviour of sand waves (Németh, 2003).

Furthermore, we investigated the results for small amplitude sand waves under a steady flow only. It has been shown that with a set up describing sand waves in a tidal environment, we find bed features existing in a unidirectional steady current similar to *dunes*. These dune-like bed forms are found when the roughness of the seabed, compared to a typical North Sea situation, is large. For smaller values of the resistance of the seabed, taken into account by the resistance parameter S, the instability mechanism is very weak, resulting in a FGM with very long wavelengths.

Lastly, the numerical approach presented here enables us to incorporate more realistic aspects into the modelling framework. It is clear that the simulation model presented here can straightforwardly be extended to include other aspects such as a critical shear stress, suspended sediment transport or a non-erodible layer in the seabed.

Acknowledgements

This work is supported by Technology Foundation STW, the applied science division of NWO and the technology programme of the Ministry of Economic Affairs and performed within the EU-sponsored project HUMOR (HUman interaction with large-scale coastal MORphologic evolution; EVK3-CT-2000-00037). Furthermore, we would like to thank Huib de Vriend for the discussions and his advice.

Appendix A

The two-dimensional version of the derivative matrix $\mathbf{D}$ in Eq. (14) in the horizontal direction can be written with the derivative matrix $\mathbf{D}$ of the size $N^1\times N^1$ as N^3 blocks on the diagonal of the following square matrix with $N^1\times N^3$ columns:

$$\mathbf{D}^1=\begin{pmatrix} \mathbf{D}^1_{11} & \cdots & D^1_{1N} & & & & & & \\ \vdots & \ddots & \vdots & & & & & 0 & \\ \mathbf{D}^1_{N1} & \cdots & \mathbf{D}^1_{NN} & & & & & & \\ & & & \mathbf{D}^1_{11} & \cdots & \mathbf{D}^1_{1N} & & & \\ & & & \vdots & \ddots & \vdots & & & \\ & & & \mathbf{D}^1_{N1} & \cdots & \mathbf{D}^1_{NN} & & & \\ & & & & & & \mathbf{D}^1_{11} & \cdots & \mathbf{D}^1_{1N} \\ & 0 & & & & & \vdots & \ddots & \vdots \\ & & & & & & \mathbf{D}^1_{N1} & \cdots & \mathrm{D}^1_{NN} \end{pmatrix} \tag{40}$$

The rest of the elements are zero. The two-dimensional version of the derivative matrix $\mathbf{D}$ in Eq. (14) with size $N^3\times N^3$ to determine derivatives in the vertical direction can be written

as the elements of $\mathbf{D}^3$ in a diagonal pattern with a spacing of N^1 elements as follows:

$$\mathbf{D}^3 = \begin{pmatrix} \mathbf{D}^3_{11} & & 0 & & \mathbf{D}^3_{12} & & 0 & & \mathbf{D}^3_{1N} & & 0 \\ & \ddots & & & & \ddots & & & & \ddots & \\ 0 & & \mathbf{D}^3_{11} & & 0 & & \mathbf{D}^3_{1j} & & 0 & & \mathbf{D}^3_{1N} \\ \mathbf{D}^3_{i1} & & 0 & & \mathbf{D}^3_{ij} & & 0 & & \mathbf{D}^3_{iN} & & 0 \\ & \ddots & & & & \ddots & & & & \ddots & \\ 0 & & \mathbf{D}^3_{i1} & & 0 & & \mathbf{D}^3_{ij} & & 0 & & \mathbf{D}^3_{iN} \\ \mathbf{D}^3_{N1} & & 0 & & \mathbf{D}^3_{Nj} & & 0 & & \mathbf{D}^3_{NN} & & 0 \\ & \ddots & & & & \ddots & & & & \ddots & \\ 0 & & \mathbf{D}^3_{N1} & & 0 & & \mathbf{D}^3_{Nj} & & 0 & & \mathrm{D}^3_{NN}, \end{pmatrix} \tag{41}$$

The rest of the elements are zero.

The matrix below with a total size of $N^1 \times N^3 \times 2 + N^1 \times 2$ can be found in Eq. (22) and consist of the variables depending on time in the momentum equation Eq. (1) (the first $N^1 \times N^3$ rows), the continuity equation (Eq. (2)) giving elements equal to zero (the next $N^1 \times N^3$ rows), and the equation for the water level Eq. (6) and the bed evolution Eq. (8) ($2 \times N^1$ rows). For the water level, we use the kinematic boundary condition at the free surface. This is equivalent to using a depth-averaged formulation based on the continuity equation and this kinematic boundary condition often used to describe a free surface:

$$A = \begin{pmatrix} \frac{\partial u}{\partial t} & 0 & f\left(\frac{\partial \zeta}{\partial t}\right) & f\left(\frac{\partial h}{\partial t}\right) \\ 0 & 0 & 0 & 0 \\ 0 & 0 & \frac{\partial \zeta}{\partial t} & 0 \\ 0 & 0 & 0 & \frac{\partial h}{\partial t} \end{pmatrix} \tag{42}$$

See Eq. (23) for the numerical notation.

References

Allen, J.R.L., 1980a. Sand waves: a model of origin and internal structure. Sediment. Geol. 26, 281–328.

Allen, J.R.L., 1980b. Sand wave immobility and the internal master bedding of sand wave deposits. Geol. Mag. 117 (5), 347–446.

Besio, G., Blondeaux, P., 2003. On the effect of the suspended load on the formation of sand waves. In: Sanchez-Arcilla, A., Bateman, A. (Eds.), RCEM 2003, Proceedings Third IAHR Symposium on River, Coastal and Estuarine Morphodynamics. Spain, IHAR, Madrid, pp. 365–375.

Besio, G., Blondeaux, P., Brocchini, M., Vittori, G., 2003. Migrating sand waves. Ocean Dyn. 53, 232–238.

Besio, G., Blondeaux, P., Brocchini, M., Vittori, G., 2004. On the modeling of sand wave migration. J. Geophys. Res. 109, C04018. doi:10.1029/2002JC001622.

Canuto, C., Quarteroni, A., Yousuff Hussaini, M., 1988. Spectral Methods in Fluid Dynamics. ISBN: 0-387-17371-4.

Fornberg, B., 1996. A Practical Guide to Pseudospectral Methods, Cambridge Monographs on Applied and Computational Mathematics, vol. 1. University of Colorado, Cambridge University Press.

Fredsøe, J., Deigaard, R., 1992. Mechanics of Coastal Sediment Transport, Institute of Hydrodynamics and Hydraulic Engineering. Technical University of Denmark, pp. 260–289.

Gerkema, T., 2000. A linear stability analysis of tidally generated sand waves. J. Fluid Mech. 417, 303–322.

Hulscher, S.J.M.H., 1996. Tidal induced large-scale regular bed form patterns in a three dimensional shallow water model. J. Geophys. Res. 101 (C9), 20727–20744.

Hulscher, S.J.M.H., Van den Brink, G.M., 2001. Comparison between predicted and observed sand waves and sandbanks in the North Sea. J. Geophys. Res. 106 (C5), 9327–9338.

Huthnance, J., 1982. On one mechanism forming linear sandbanks. Estuar. Coast. Shelf Sci. 14, 79–99.

Johns, B., Soulsby, R.L., Chesher, T.J., 1990. The modelling of sand wave evolution resulting from suspended and bed load transport of sediment. J. Hydraul. Res. 28 (3), 355–374.

Johnson, M.A., Stride, A.H., Belderson, R.H., Kenyon, N.H., 1981. Predicted sand-wave formation and decay on a large offshore tidal-current sand-sheet. Spec. Publ. Int. Assoc. Sedimentol. 5, 247–256.

Knaapen, M.A.F., Hulscher, S.J.M.H., 2002. Regeneration of dredged sand waves. Coast. Eng. 46 (4), 277–289.

Komarova, N.L., Hulscher, S.J.M.H., 2000. Linear instability mechanisms for sand wave formation. J. Fluid Mech. 413, 219–246.

Komarova, N.L., Newell, A.C., 2000. Non-linear dynamics of sandbanks and sand waves. J. Fluid Mech. 415, 285–321.

Lanckneus, J., De Moor, G., 1991. Present-day Evolution of Sand Waves on a Sandy Shelf Bank, Oceanologica Acta, Proceedings of the International Colloquium on the Environment of Epicontinental seas, *Lille*, sp vol. 11, pp. 123–127.

Langhorne, D.N., 1981. An evaluation of Bagnolds dimensionless coefficient of proportionality using measurements of sand wave movements. Mar. Geol. 43, 49–64.

Morelissen, R., Hulscher, S.J.M.H., Knaapen, M.A.F., Németh, A.A., Bijker, R., 2003. Interacting sand waves and pipelines: a data-assimilation based mathematical model. Coast. Eng. 48 (3), 197–209.

Németh, A.A., 2003. Modelling offshore sand waves, Ph.D. thesis, University of Twente, The Netherlands (ISBN 90-365-1931-4).

Németh, A.A., Hulscher, S.J.M.H., Van Damme, R.M.J., 2001. Numerical simulation of sand wave evolution in shallow shelf seas. In: Hanson, H., Larson, M. (Eds.), Proceedings of the Fourth Conference on Coastal Dynamics, Lund, Sweden, pp. 1048–1057.

Németh, A.A., Hulscher, S.J.M.H., de Vriend, H.J., 2002. Modelling sand wave migration in shallow shelf seas. Cont. Shelf Res. 22 (18–19), 2795–2806.

Peters, B.G.T.M., Hulscher, S.J.M.H., Roos, P.C., 2001. Large-scale sand extraction offshore: interacting between model and decision process. FOMAR.-Congreso International Cienca Y Technologia Marina, April 24–27th, Spain.

Stelling, G., Roose, D., Sommeijer, B.P., Houwen, P.J., Kok, J., Lin, H.X., Tan, K., 1998. New generation shelf flux models. Modelling, Analysis and Simulation (MAS) MAS-R9815. Report MAS-R9815. CWI, The Netherlands p. 32.

Stolk, A., 2000. The role of sandwaves in the management of the Netherlands Continental Shelf. In: Trentesaux, A., Garlan, T. (Eds.), Marine Sandwave Dynamics, International Workshop, March 23–24 2000, University of Lille 1, France, Proceedings, pp. 93–197.

Van Maren, D.S., 1998. Sand Waves, A State-of-the-Art Review and Bibliography. North Sea Directorate, Ministry of Transport, Public Works and Water Management, The Netherlands. 118 pp.

Van Rijn, L.C., 1993. Handbook of sediment transport by currents and waves. Delft Hydraulics, Delft, The Netherlands.